Abusive Head Trauma: Developing a Computational Adult Head Model to Predict Brain Deformations under Mild Accelerations

Nikini T. Puhulwelle Gamage, Andrew K. Knutsen, Dzung L. Pham, Andrew J. Taberner, Martyn P. Nash, and Poul M.F. Nielsen

1 Introduction

"Shaken baby syndrome" (SBS) is a well-known phrase used to describe a class of head injuries inflicted on young infants by their caregivers. As the name implies, it was thought for many years that these injuries were caused by violent shaking. However, it is now recognised that mechanisms involving impact may cause very similar injuries and hence the term "Abusive Head Trauma" (AHT) is now used, which does not require the medical practitioner to assume one specific mechanism of injury [1].

The injuries most commonly associated with AHT include intracranial bleeding (typically subdural) and bleeding into the retina, although a variety of other injuries may be sustained [2]. These injuries are not visible externally. Therefore, for a head injury to be diagnosed in an infant with no external signs of trauma, the infant must present symptoms of brain dysfunction (encephalopathy). These symptoms can be subtle, and vary from vomiting and lethargy to coma and acute collapse [3]. Internationally, the incidence of AHT is between 14 and 40 per year per 100,000 infants under the age of one [4].

N.T. Puhulwelle Gamage
Auckland Bioengineering Institute, The University of Auckland, Auckland, New Zealand

A.K. Knutsen • D.L. Pham
Center for Neuroscience and Regenerative Medicine, The Henry M. Jackson Foundation, Bethesda, MD, USA

A.J. Taberner • M.P. Nash • P.M.F. Nielsen (✉)
Auckland Bioengineering Institute, The University of Auckland, Auckland, New Zealand

Department of Engineering Science, The University of Auckland, Auckland, New Zealand
e-mail: p.nielsen@auckland.ac.nz

Uncertainties about the mechanisms of injury often become a central issue in criminal trials. This is particularly so for infants with no external signs of impact and no fractures of the ribs or long bones. In these infants, the classical "shaken babies", it may be argued that there was no trauma at all. In particular, it is often argued that shaking alone cannot cause serious brain injuries, and that the whole concept of SBS is fundamentally flawed. In these arguments, the lack of biomechanical evidence for shaking as a cause of injury often plays a key role [5]. It has become clear that further biomechanical research is needed to help determine the quantitative linkages between shaking an infant and the injuries that may result. Computational modelling of the infant head can help to address ambiguities surrounding the diagnosis of AHT.

The main aim of the AHT research project at the Auckland Bioengineering Institute is to ascertain if shaking alone can cause the injuries seen in AHT. In order to address this question, the problem has been separated into three parts. The first was to determine the mechanical coupling between the torso and the head. This involved determining how the head moved when the torso was shaken [6]. The second part was to use measurements of head motions to investigate the mechanical effects on the infant brain under these conditions. The third part was to link the mechanical indices identified and link them to the injuries seen in AHT.

In order to create an accurate computational infant head model the computational techniques used to create this model need to be validated. This paper outlines how an adult head model was created and validated using in-vivo experimental data. The computational techniques that were validated in this paper will then be used to create an infant head model, which could then be used to determine certain mechanical indices on the infant brain under a shaking motion.

2 Methods

A set of mild acceleration in-vivo adult head rotation experiments were conducted. The deformations of the brain under these rotational motions were measured and were used to validate a finite element (FE) model.

A healthy volunteer was placed supine into a magnetic resonance imaging (MRI) scanner with a rotational rig placed around their head. When a pulley was actuated, a latch was released allowing the head to rotate approximately 30°, guided by an off axis weight until a mechanical stop was reached. This protocol provided repeatable accelerations of approximately 260 rad·s^{-2}. These experiments were approved by the Internal Review Board at the National Institute of Health (USA) [7].

Tagged MR images were acquired using a novel approach that combined a modified tagged MRI pulse sequence with an MRI-compatible angular position sensor [7]. The imaging and the rotation were synchronised using a fibre optic sensor, which detected the release of the latch and started the MRI sequence. The tag lines were applied immediately at the start of the motion, and a second trigger was sent to the scanner when the shaft of the device rotated through approximately 29°,

Fig. 1 The rotational displacement of the adult head. The first (*left*) *red line* shows when the data started to be acquired and the second (*right*) *red line* shows the end of the data acquisition
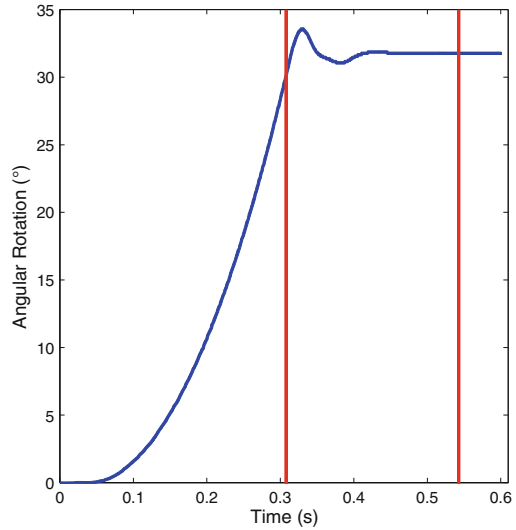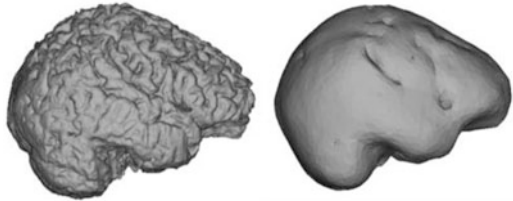

Fig. 2 *Left*: the original STL surface mesh that was obtained from ITK Snap. *Right*: the STL mesh after it had been modified with MeshLab

beginning the cine gradient echo acquisition from which the displacements were obtained.

To capture the full deformation of the brain, the experiments were repeated 120 times. Image displacements were computed using harmonic phase (HARP) analysis [8]. A filter radius was applied to create the HARP images. Two dimensional displacements of 14 axial slices throughout the adult brain were obtained. Starting at the base of the brain (brainstem), slices were regularly spaced at 10 mm intervals. This resulted in 13 slices and 59,478 points of measurement. Data for 13 time steps were collected, with the acquisition starting at 0.3074 s (first red line in Fig. 1) just before the mechanical stop and data collected every 18 ms until 0.5422 s (second red line). The 2D displacements were all measured relative to the first time step.

The rotational displacement of the whole head can be seen in Fig. 1. The first peak shows when the head came to a compliant stop. Once the rig contacted this stop, it would rebound slightly—an event evident in the decaying ripple after the first peak.

To determine the experimental error, rotational experiments were conducted on a gel phantom multiple times and the displacements throughout the gel, over time were measured. The variation in these results showed an experimental precision

error (uncertainty) of 1.5 mm. The bias error (accuracy) was not determined from these experiments. However, very low bias errors have been shown to occur for a similar MR imaging technique [9]. Therefore an experimental error of 1.5 mm will be used when analysing the results.

A computational FE model of the adult head undergoing mild acceleration rotational motions was created with ANSYS Workbench, using a fluid–structure interaction (FSI) model. A high resolution MR scan of the geometry of the volunteer's head was imported into the ANSYS Workbench environment. Volumes corresponding to the brain, brain stem, and the optic nerves of the volunteer were segmented from the model. ITK Snap (US National Institute of Health, [10]) was used to segment the images using active contour segmentation. This is a semi-automated segmentation process, where certain sections of the head could be segmented based on intensity levels, expansion force, smoothing force, and edge attraction force [10]. The segmented images were subsequently cleaned manually.

The cerebrospinal fluid (CSF) and the skull were not segmented from the MR images as the T1 weighted MRI intensity levels of the skull and the CSF could not be differentiated. Gravitational loading while the brain was being imaged could also alter the volume of the CSF. Because of this the CSF and skull had to be created manually. Once the entire brain had been segmented, the data were written to stereolithography (STL) files and imported into MeshLab (National Research Council (Italy)), a 3D mesh processing application. The STL surface mesh that was obtained from ITK Snap was cleaned, filtered, and reduced using MeshLab (see Fig. 2).

This processing of the initial STL mesh resulted in the fine folds of the brain (gyri and sulci) being smoothed out. This was acceptable as these folds were not thought to substantially influence the mechanical behaviour of the brain, but would overly complicate the final FE mesh geometry. This processing did cause the dimensions of the brain to decrease by approximately 2 mm in height and length. The STL files for the brain stem and the optic nerve were not processed in this way as they did not contain a complex outer surface.

Once the cleaned STL files had been created, they were saved as a ".XYZ" file, which contained the locations of all the nodes and the surface normals. The XYZ file of the brain was then used to create the CSF and skull of the adult head. MATLAB (The Math Works Inc., 2013) was used to project the nodes outwards to create the outer surface of the CSF layer and further extended to create the outer surface of the skull. The geometric models of the CSF and the skull were then saved as ".XYZ" files. MeshLab was used to create the outer surfaces of the CSF and the skull from the nodes and the surface normals. A Poisson surface reconstruction algorithm was used to create the surface from the point clouds. This model contained a 2 mm CSF layer and a 6 mm thick skull [11].

The falx cerebri and the tentorium cerebelli were added to the existing geometry. These structures could not be segmented using ITK Snap as they had similar MRI intensities as the surrounding tissue; instead, these structures were added manually using ANSYS ICEM (ANSYS Inc., Canonsburg, PA, USA). The outlines of the falx and tentorium were created using points and line segments. Faces were then inserted to create a final geometry. The longitudinal fissure and the transverse fissure were

Fig. 3 The volume mesh of the adult head. *Top left*: transverse plane, *Top right*: Off-centred medial plane, *Bottom left*: Isometric view, *Bottom right*: Coronal plane. *Red* represented the brain, *blue* the CSF, green the skull, and pink the falx and tentorium
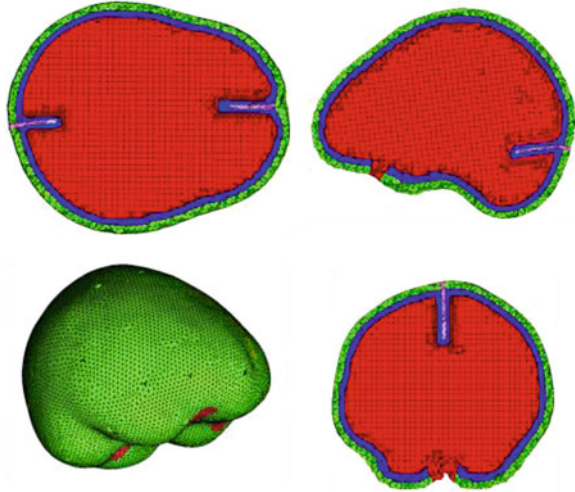
used to position the falx and the tentorium at the correct positions. These surfaces were also projected outwards by 2 mm to create the CSF layer between the brain and the falx cerebri and the tentorium cerebelli. The sizes of the falx cerebri and the tentorium cerebelli were estimated from the MRI scans and were consistent with those reported in the literature [11].

Once the anatomical surface model was created, a volume mesh was built using ANSYS ICEM. All surface meshes were imported into ICEM and an integrated volumetric mesh was created through an automated process. Tetrahedral meshes were used for the skull, CSF, falx, tentorium, optic nerves, and brainstem. The surface of the brain was described using tetrahedral elements. The main body of the brain was meshed using a hexahedral mesh. Figure 3 shows the mesh that was created by ICEM. The structural mesh (everything apart from the CSF) contained 24,831 elements, while the fluid component contained 85,504 elements. Once the geometry had been discretised, it was imported into ANSYS Workbench.

This workflow resulted in a model where the brain was contained inside a skull and surrounded by a 2 mm thick CSF layer. The falx cerebri and the tentorium cerebelli protruded into the skull, thereby separating the two hemispheres of the brain and the cerebellum. CSF was also present between the falx and brain, and between the tentorium and the brain. The optic nerves and the brainstem tether the brain to the skull, and both extend from the brain through the CSF to the outer surface of the skull. This arrangement is illustrated in Fig. 3, where the green elements represent the skull, blue elements represent the CSF, pink elements represent the falx and tentorium, and red elements represent the brain.

Table 1 lists the material properties that were assigned to each part of the model. The outer skull, falx, and tentorium were modelled using elastic material properties. The CSF was modelled using the standard fluid properties of density (ρ) and viscosity (η). The brain, optic nerves, and brainstem were modelled using a linear viscoelastic material property.

Table 1 The material properties that were used in the computational model

Anatomical structure	Material model
Brain	$G_0 = 0.038$ MPa, $G_\infty = 0.007$ MPa, $t_I = 0.0014$ s [12–15]
Skull	$E = 7$ GPa, $\mu = 0.22$ [16, 17]
CSF	$P = 1000.59$ kgm^{-3}, $\eta = 0.78$ [18–20]
Falx/Tentorium	$E = 31.5$ MPa, $\mu = 0.23$ [14, 15, 21]

The rotational displacement of the head (Fig. 1) was used as a kinematic constraint on the FE model and was applied to the outer nodes of the skull. Two sets of contact conditions were applied in this model. A bonded contact condition was implemented between the outer edge of the optic nerves and the skull, and a frictionless contact condition was applied between the brainstem and the skull. The frictionless contact condition allowed the brainstem to move independently of the skull and the bonded contact condition of the optic nerve did not let the optic nerve to move independently of the skull. These constraints were assumed to provide a reasonable representation of the interactions between these anatomical structures. An FSI boundary was placed on the outer surface of the brain and the inner surface of the skull. This allowed the displacements from the solid solver to be transferred to the fluid domain (CSF) and the forces from the fluid solver were transferred to the solid domain (brain and skull). This was a simplified representation of the meninges layers but this proved to be sufficient to accurately model the deformation of the brain under mild angular rotations.

3 Results

The results from the FE model and the experimental model were compared to determine whether the FE model could reliably represent the deformation of the brain. Figure 4 shows the root mean squared (RMS) error between the resultant displacements magnitudes between all the points (59478) measured from the adult experiments and the predicted displacements from the corresponding points in the computational model. The time steps relate to the acquisition time of the tagged MRI images. The RMS error was seen to vary with the rotation of the brain.

Figure 5 shows the magnitude of the displacements and the errors associated at each time point. The error was calculated by taking the absolute differences between the measured and the predicted displacements. There was no obvious relationship between the absolute errors and the total displacement of the brain.

Figure 6 shows the relative errors between the measured and the predicted displacements. The relative errors were calculated by dividing the absolute differences between the measured and predicted displacements by the measured displacements. Time steps 2, 3, 4, and 6 have median relative errors below 0.1 and the other time steps had median relative errors that were above 0.1.
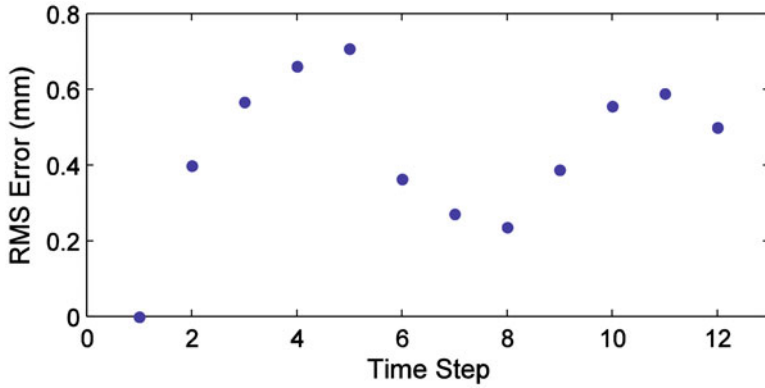
Fig. 4 RMS error between the experimental data and the FE model for each time step for the adult head model. The time steps were 18 ms apart from one another
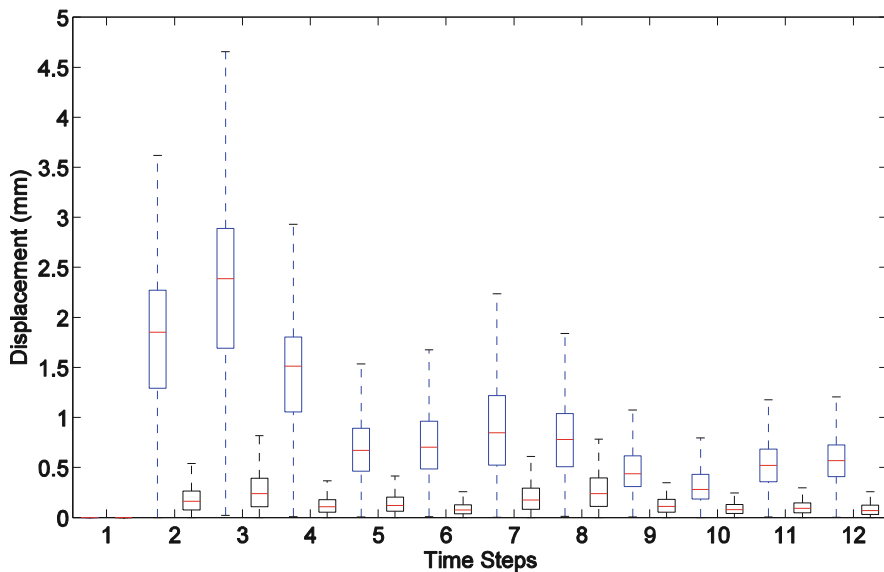

Fig. 5 Shows the displacement magnitudes (*blue*) from the measured displacement for each time step and the absolute errors (*black*) between the measured and the predicted displacement values. The time steps were 18 ms apart from one another

Figure 7 shows a slice (coronal plane of the brain) of the raw data from the experimental results (left), the FE model (middle), and their difference (right). The colours in these plots represent the x displacement (perpendicular to the plane shown) of the brain, with maximum value of 3.4 mm (red) and a minimum of -4.2 mm (blue). All the displacements measured were relative to the first time step. The following time steps show the displacement of the brain from just after the head
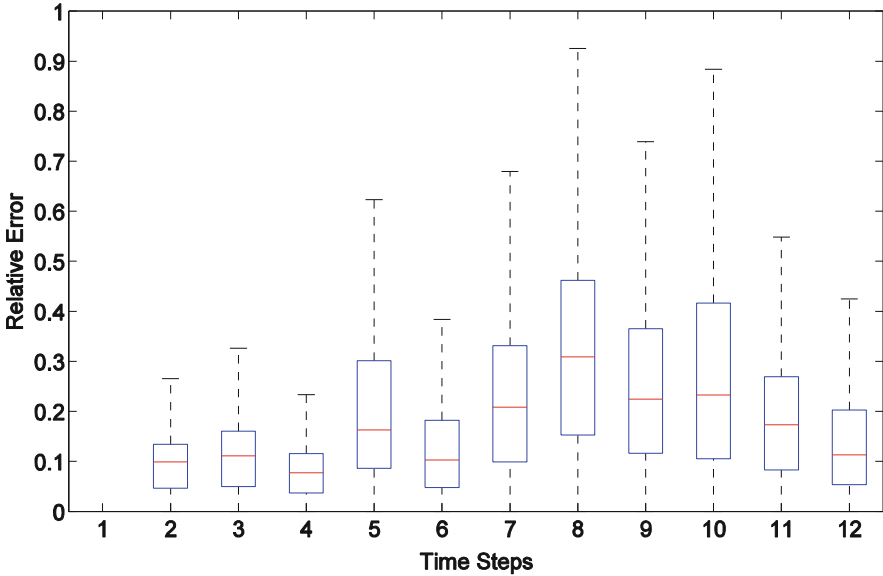
Fig. 6 Relative errors between the predicted and the measured displacements at each of the time steps, the time steps were 18 ms apart from one another

had hit a mechanical stop. The brain deforms the greatest amount during the start and settles as the experiments go on. Only the first six time steps are shown as the deformations were small in the remaining time steps.

4   Discussion

The main aim of this work was to validate a computational model that was used to predict the displacements of the adult human brain undergoing mild rotational accelerations. A volunteer underwent mild acceleration (max of 260 rad·s^{-2}) head rotations, where the 3D deformation of the brain was measured using a tagged MRI sequence. The motion of the volunteer's head was recorded and the rotational displacements were used to kinematically constrain the outer nodes of the FE model of the skull. The displacements of the brain under this rotation predicted by the FE model were compared to the displacements measured in the experiment.

The maximum and RMS error between the predicted displacements and the measured displacements at each time step are presented in Fig. 4. All RMS errors were below the experimental error of 1.5 mm. Thus, the FE model provides acceptable predictive accuracy.

A comparison of the measured displacements and the prediction errors is illustrated in Fig. 5. Acquisition commenced immediately prior to the impact with
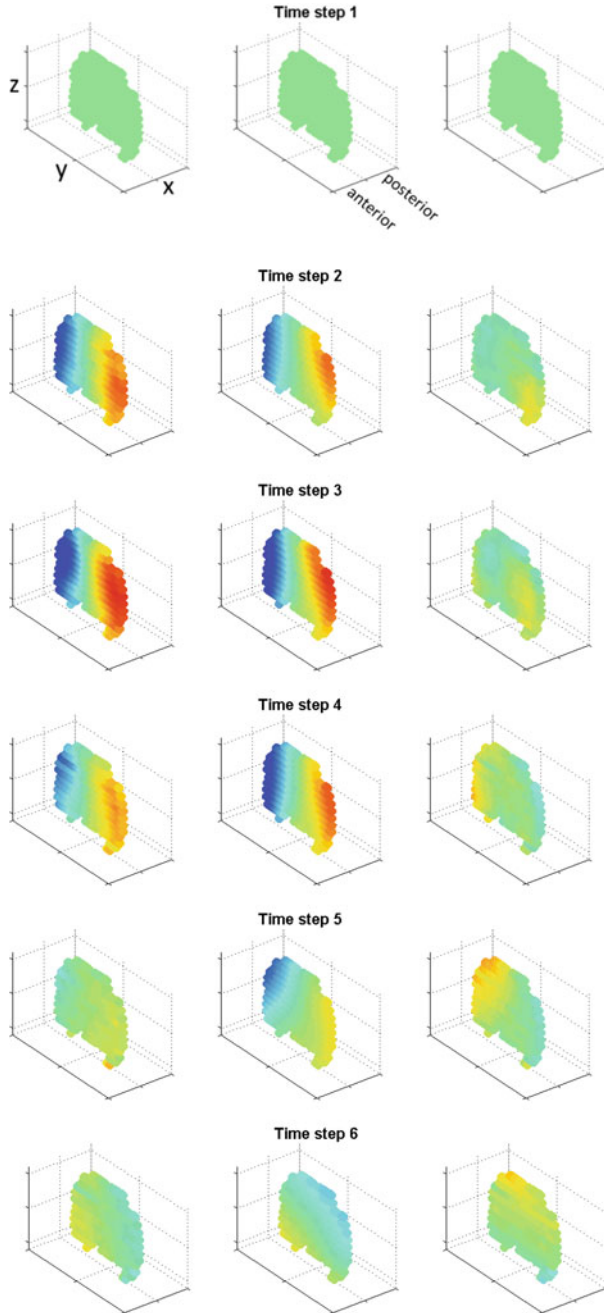
Fig. 7 Comparison of x-displacements from the experiments (*left*) and the FE model (*middle*), with the difference between the two (*right*), for the adult head FE model. The colours in these plots represent the *x* displacement of the brain, with maximum value of 3.4 mm (*red*) and a minimum of −4.2 mm (*blue*)

the mechanical stop, in order to capture the maximum displacements of the brain. This is evident as the first three time steps had median displacements of more than 1.5 mm. When the head ceased rotating, and the brain motion settled, the median displacements measured were below 1 mm. The median absolute error in the model predictions were below 0.3 mm, which was well below the experimental error, and much smaller than the overall displacement of the brain. The absolute errors were also relatively constant throughout the rotation of the head. Figure 7 also conveys this information. The relative errors between the predicted and the measured displacements at each of the time steps (Fig. 6) were small for time steps 2, 3, and 4. However, there were rather large relative errors at other time points. This was because of the small displacements (medians lower than 1 mm) at these time steps coupled with the relatively constant absolute errors throughout the experiment. This combination would result in a high relative error and hence these errors do not detract anything from the predictive capabilities of the computational model. These results provide confidence in the computational model that was used to predict the displacement of the brain under mild acceleration rotations.

This paper has detailed the construction of an FE model that was used to predict the displacements of the adult human brain undergoing mild rotational accelerations. The computational techniques required to predict the displacement of the brain were validated using in-vivo measurements of human brain displacements. In future, these computational techniques will be incorporated into an FE model of an infant head in order to predict the mechanical effects on the infant brain under a shaking motion. The dynamic stresses, strains, and the motion of the brain in relation to the skull will be used to help ascertain whether injuries could result from particular shaking incidents.

References

1. Christian CW, Block R (2009) Abusive head trauma in infants and children. Pediatrics 123:1409–1411
2. Chiesa A, Duhaime A-C (2009) Abusive head trauma. Pediatr Clin N Am 56:317–331
3. Minns R, Busuttil A (2004) Patterns of presentation of the shaken baby syndrome. Br Med J 328:766
4. Sieswerda-Hoogendoorn T, Boos S, Spivack B, Bilo RA, van Rijn RR (2012) Educational paper: abusive head trauma part I. Clinical aspects. Eur J Pediatr 171:415–423
5. Tuerkheimer D (2009) The next innocent project: shaken baby syndrome and the criminal courts. Washingt Univ Law Rev 87(1):1–58
6. Lintern TO (2014) Modelling infant head kinematics in abusive head trauma. Doctoral thesis, University of Auckland, Auckland, New Zealand. Retrieved from http://hdl.handle.net/2292/22988

7. Knutsen AK, Magrath E, McEntee JE, Xing F, Prince JL, Bayly PV, Butman JA, Pham DL (2014) Improved measurement of brain deformation during mild head acceleration using a novel tagged MRI sequence. J Biomech 47:3475–3481

8. Osman NF, Kerwin WS, McVeigh ER, Prince JL (1999) Cardiac motion tracking using CINE harmonic phase (HARP) magnetic resonance imaging. Magn Reson Med 42:1048–1060

9. Bayly P, Ji S, Song S, Okamoto R, Massouros P (2004) Measurement of strain in physical models of brain injury: a method based on HARP analysis of tagged magnetic resonance images (MRI). J Biomech Eng 126(4):523–528

10. Yushkevich PA, Piven J, Hazlett HC, Smith RG, Ho S, Gee JC, Gerig G (2006) User-guided 3D active contour segmentation of anatomical structures: significantly improved efficiency and reliability. NeuroImage 31:1116–1128

11. Hiatt JL, Gartner LP (2009) Textbook of head and neck anatomy. Lippincott Williams and Wilkins, Philadelphia

12. Al-Bsharat AS (2000) Computational analysis of brain injury. Doctoral thesis, Wayne State University, MI, USA. Retrieved from http://elibrary.wayne.edu/record=b2760872~S47

13. Chen Y (2011) Biomechanical analysis of traumatic brain injury by MRI-based finite element modeling. Doctoral thesis, University of Illinois, Champaign, IL, USA. Retrieved from https://www.ideals.illinois.edu/bitstream/handle/2142/29640/CHEN_YING.pdf?sequence=1

14. Tse KM, Lim SP, Tan VC, Lee HP (2014) A review of head injury and finite element head models. Am J Eng Technol Soc 1:28–52

15. Zhang L, Yang KH, King AI (2001) Comparison of brain responses between frontal and lateral impacts by finite element modeling. J Neurotrauma 18:21–30

16. Zoghi-Moghadam M, Sadegh AM (2009) Global/local head models to analyse cerebral blood vessel rupture leading to ASDH and SAH. Comput Methods Biomech Biomed Engin 12:1–12

17. Horgan TJ, Gilchrist MD (2004) Influence of FE model variability in predicting brain motion and intracranial pressure changes in head impact simulations. Int J Crashworthiness 9:401–418

18. Brydon HL, Hayward R, Harkness W, Bayston R (1995) Physical properties of cerebrospinal fluid of relevance to shunt function. 1: the effect of protein upon CSF viscosity. Br J Neurosurg 9:639–644

19. Bloomfielda IG, Johnstona IH, Bilstonb LE (1998) Effects of proteins, blood cells and glucose on the viscosity of cerebrospinal fluid. Pediatr Neurosurg 28:246–251

20. Kuchuk VI, Shirokova IY, Golikova EV (2012) Physicochemical properties of water-alcohol mixtures of a homological series of lower aliphatic alcohols. Glas Phys Chem 38:460–465

21. Willinger R, Kang HS, Diaw B (1999) Three-dimensional human head finite-element model validation against two experimental impacts. Ann Biomed Eng 27:403–410